Journal of Materials Chemistry

Cite this: *J. Mater. Chem.*, 2012, **22**, 20881

www.rsc.org/materials

COMMUNICATION

Anomalous energy-gap behaviour of armchair BC_3 ribbons due to enhanced π-conjugation

Sudipta Dutta and Katsunori Wakabayashi*

Received 24th July 2012, Accepted 23rd August 2012
DOI: 10.1039/c2jm34881k

The effect of edge passivation on armchair BC_3 ribbons is studied by first-principles calculations. The removal of passivating hydrogen from the edge boron atoms provides higher stability and makes the narrower ribbons metallic due to the enhanced π-conjugation along the edge. However, an increase in the ribbon width results in an unprecedented metal-to-semiconductor transition.

The remarkable electronic properties of graphene[1–3] have inspired the exploration of other atomically thin materials, such as silicene,[4,5] hexagonal boron nitride (h-BN),[6] MoS_2,[7,8] and BC_3,[9–11] in the search for additional functionalities: enhanced spin–orbit coupling,[12,13] strong electronic correlation,[14,15] high-κ dielectrics[16] and a semiconducting energy gap.[11,17] A hybrid system composed of these different two-dimensional materials with graphene can be designed to tune the electronic properties,[18,19] *e.g.*, graphene on an h-BN substrate can be used to realise the enhanced electron mobility and fractional quantum Hall effect of graphene.[20] Optical devices using these hybrid structures have also been proposed.[21] Furthermore, these low-dimensional materials exhibit dominant edge effects that can be manipulated to obtain exotic electronic,[22–24] magnetic[25,26] and transport properties.[27]

Currently, passivating the edges with hydrogen atoms has been a common trend in the theoretical approaches to satisfy the dangling bonds.[28,29] In the case of graphene nanoribbons, the electronic states that result from the addition of hydrogen appear far from the Fermi energy level and cannot alter the electronic properties. However, in other two-dimensional materials, the addition of hydrogen atoms can cause dramatic changes because of the modified hybrid orbitals. In this communication, we address the effect of edge passivation using BC_3 as an example.

Our theoretical investigations based on *ab initio* calculations[30] demonstrate how the absence of hydrogen passivation on the boron atoms modifies the hybridisation and stabilises the armchair BC_3 ribbons, which makes the narrower ribbons metallic. However, the anomalous behaviour of band-gap opening occurs for wider ribbons.

BC_3 consists of a two-dimensional honeycomb lattice with a homogeneous distribution of boron atoms. Unlike graphene, where the π-electrons are delocalised over the entire lattice, BC_3 presents a Kekulé-like structure with aromatic carbon hexagons with a π-electron on each carbon atom, which are separated by anti-aromatic hexagons consisting of carbon and boron atoms,[31] as can be seen from the charge density distribution plot in Fig. 1a. This structure has been predicted to be the most stable compared to other possible structures with different distributions of boron atoms within the honeycomb lattice.[32] The experimental fabrication of a BC_3 sheet over a NbB_2 (0001) surface *via* carbon substitution in the boron honeycomb layer of metal diboride by C. Oshima and co-workers supports the theoretical prediction.[9,10]

The band structure and the density of states (DOS) of the BC_3 sheet shown in Fig. 1b exhibit a finite indirect band gap, which has also been previously observed within various levels of theoretical frameworks.[11,33] This finite gap in BC_3 provides an advantage over the metallic graphene for device applications. As we know, doping boron into graphene systems introduces holes,[34] shifting the Fermi energy level to a lower energy. Therefore, the Dirac cone, which is a characteristic signature of graphene, remains above the Fermi energy level in the case of a BC_3 sheet (see Fig. 1b). Furthermore, the valence bands constructed by the σ orbitals move closer to the Fermi energy level (see Fig. 1b).

Depending on the terminations, the BC_3 sheet can produce three distinct classes of armchair edge geometries: (i) C–C dimer lines in both edges (Fig. 1c), (ii) C–B dimer lines in both edges (Fig. 1d) and (iii) C–C and C–B dimer lines in either edge (Fig. 1e). The width of the armchair BC_3 ribbons is defined by the "N_a" index, where "N" is the number of dimer lines along the cross-ribbon width direction. For the first two classes of armchair ribbons, N is always odd, unlike the last class, for which N is even. Note that all of the edge atoms of these three ribbons are passivated by hydrogen, which results in the edge boron atoms being devoid of any π-electrons, as it is in the bulk. However, each carbon atom contains one π-electron throughout the entire ribbon maintaining the Kekulé structure of the BC_3 sheet.

Each of these three ribbons exhibit a finite band gap that is larger than the BC_3 sheet (see Fig. 1f–h), which decreases with an increase in width[35] and approaches the bulk BC_3 gap, as can be seen in Fig. 1i. This phenomenon of an inverse width dependence of the band gap is quite common because the enhanced quantum confinement in a reduced length scale widens the gap. The relative ordering of the σ- and π-bands around the Fermi energy level at the Γ point of the BC_3 sheet remains unaltered in these ribbons, which can be seen in the band structure plots. Note that the classification of the three

International Center for Materials Nanoarchitechtonics (WPI-MANA), National Institute for Materials Science (NIMS), Namiki 1-1, Tsukuba, Ibaraki – 305-0044, Japan. E-mail: WAKABAYASHI.Katsunori@nims.go.jp; Fax: +81 29 860 4706; Tel: +81 29 860 4840

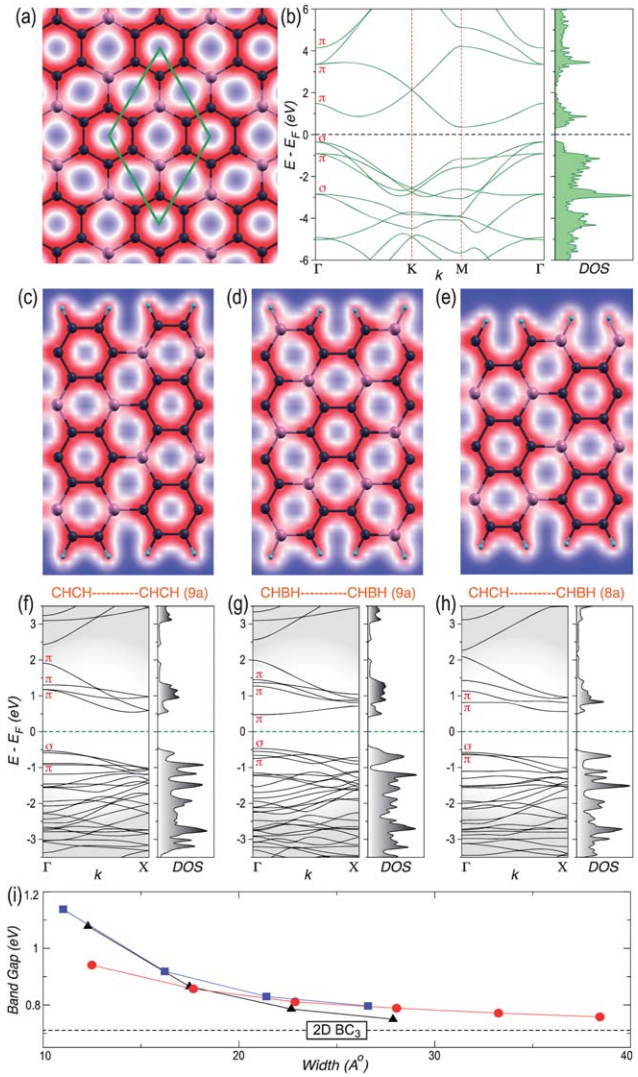

Fig. 1 (a) The optimised geometry with a rhombus unit cell containing eight atoms and the charge density plot of the BC_3 sheet revealing the Kekulé-like structure with localised electron density on the carbon hexagons. (b) The band structure and DOS of the BC_3 sheet. (c), (d) and (e) show the optimised unit cell with charge density plots for the armchair ribbons with C–C dimer lines in both edges, C–B dimer lines in both edges and C–C and C–B dimer lines in either edge, respectively, with hydrogen passivation of all edge atoms. The width of these ribbons is defined as N_a, where $N = 9, 9$, and 8, respectively. The band structure and DOS of these ribbons are shown in (f), (g) and (h), respectively, with σ and π notations showing the nature of the bands. (i) The band gap of these three classes of ribbons are shown by solid lines with closed triangles, circles and squares, respectively, as a function of width, along with that of the BC_3 sheet (dashed line).

different armchair graphene nanoribbons based on their gaps, which is regulated by the number of dimer lines along their width, does not hold true in the case of armchair BC_3 ribbons because of the downward shift of the Fermi energy level.

The origin of the gap in these classes of materials can be attributed to the localisation of π-electron clouds in the Kekulé geometry. This fact motivates us to explore this interesting material by increasing the π-conjugation in the ribbons. This process can be performed by removing the passivating hydrogen atoms from the boron atoms on the edge of the ribbons, which makes them sp-hybridised and leaves one unhybridised π-electron. Consequently, the π-conjugation along the edge is expected to increase. However, the original sp^2-hybridisation of the boron atoms remains unaltered in the bulk, with three nearest neighbour carbon atoms.

The armchair ribbon shown in Fig. 1c does not contain boron atoms at the edge. Therefore, we consider the other two armchair ribbons, which are shown in Fig. 1d and e, to investigate the effect of removing the passivating hydrogen from the edge boron atoms, as depicted in Fig. 2a and b, respectively. The optimised geometries of these ribbons clearly reveal the straightening of the C–B–C linkage at the edge, which is a characteristic signature of sp-hybridisation for unpassivated boron atoms. The π-electron density on the C–B bonds along the edges also increases, as can be seen from the charge density plots. This scenario is also reflected in their relative stabilities.

To investigate the feasibility of forming these ribbons, we calculate the stabilisation energy as $E_{stability} = E_{total} - \Sigma_e N_e E_e$. Here, E_{total} is the total energy of the respective ribbon. N_e represents the number of each element with energy E_e for each isolated atom. Fig. 2c clearly reveals an increase in stability for the ribbons with unpassivated edge boron atoms. This result can be attributed to the increase in π-electron density on the hexagons with both carbon and boron atoms with an overall enhancement of π-conjugation along the edge. The stability increases with an increase in the width of all of the classes of armchair ribbons and approaches the stability of the BC_3 sheet (see Fig. 2c). The quantitative difference of stabilisation energies of the hydrogen passivated ribbons, as presented in ref. 35, is due to

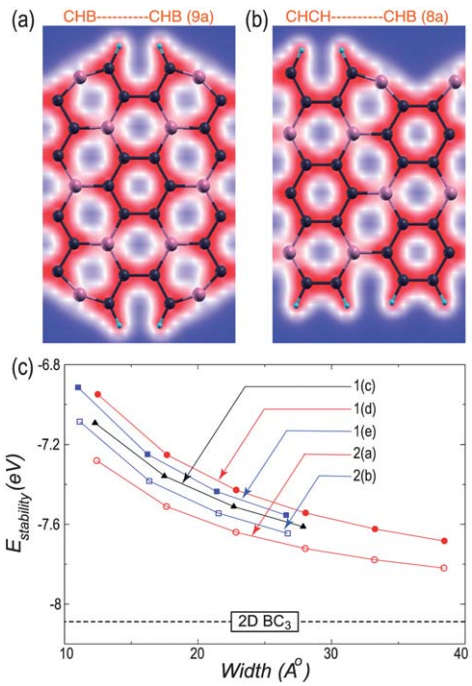

Fig. 2 (a) and (b) show the optimised unit cell with the charge density plots for the armchair ribbons with C–B dimer lines in both edges and C–C and C–B dimer lines in either edge, respectively, without passivating hydrogen atoms on the edge boron atoms. (c) Stabilisation energies ($E_{stability}$) of the armchair BC_3 ribbons shown in Fig. 1c (closed triangles), Fig. 1d (closed circles), Fig. 1e (closed squares), (a) (open circles), (b) (open squares) as a function of their width and that of the BC_3 sheet (dashed line).

different levels of calculations. However, the observation of higher stability of the ribbon in Fig. 1c compared to the BC_3 sheet in ref. 35 is in stark contrast with our results and with the common notion. This difference may be due to the lack of geometric or electronic relaxation.

We further investigate the effect of enhanced π-conjugation on the electronic properties of the armchair BC_3 ribbons with unpassivated edge boron atoms. Fig. 3a shows the band structure and the DOS for the class of ribbons depicted in Fig. 2a for different widths. We observe that, for narrower ribbons, the removal of passivating hydrogen atoms turns the semiconducting ribbons (as shown in Fig. 1i) into metallic ribbons. However, an increase in the width pushes the top of the valence band and the bottom of the conduction band apart, which opens a band gap (see Fig. 3b). This metal-to-semiconductor transition resulting from an increase in width is unprecedented in low-dimensional electronic systems. To determine the reason for this interesting phenomenon, we investigate the orbital contributions to the metallic DOS. We observe that, unlike their hydrogen-passivated counterparts, the bands around the Fermi energy level in these ribbons are constructed by the π-electrons, as can be seen from Fig. 3a. The top of the valence band and the bottom of the conduction band are primarily constructed by the π-electrons in the $2p_z$ orbitals of the unpassivated boron atoms and the subsequent atoms in the hexagons along the armchair edges, evident from their projected DOS (pDOS) plot in Fig. 3a. Therefore, the additional π-electrons in these classes of ribbons contribute to the metallic DOS. However, with an increase in width, the ratio of the edge atoms to the bulk decreases, and the effect of π-conjugation along the edge is gradually overshadowed by the bulk semiconducting property. This result is reflected in the decreased pDOS on the edges and in the gradual shift of the valence σ bands towards the Fermi energy level on an increase in width. This shift results in the anomalous behaviour of the band-gap opening upon an increase in width. The electronic structure analysis of the class of armchair BC_3 ribbons that are depicted in Fig. 2b also exhibits a similar behaviour, only with a slightly higher band gap, as shown in Fig. 3b.

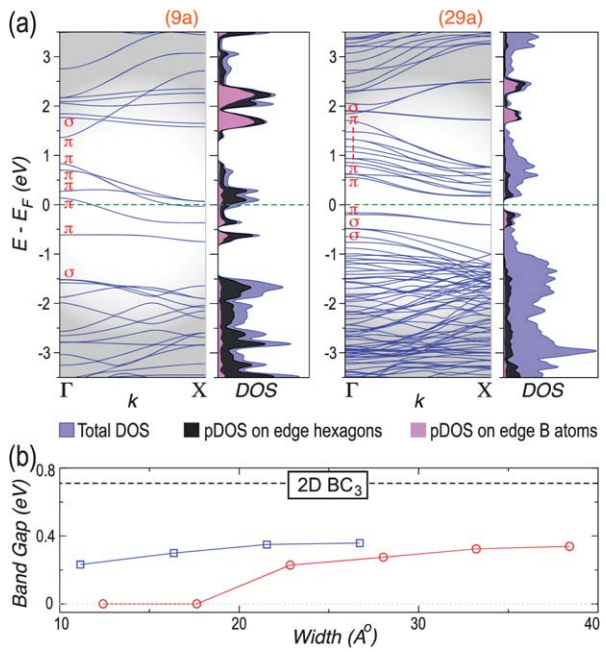

Fig. 3 (a) The band structure and DOS of the armchair ribbons with C–B dimer lines in both edges without passivating hydrogen atoms on the edge boron atoms for two different widths with $N = 9$ (left) and 29 (right). The σ and π notations are used to show the nature of the bands. The pDOS on the hexagons along the armchair edges and on the unpassivated edge boron atoms are shown along with the total DOS. (b) The band gap of the classes of armchair BC_3 ribbons shown in Fig. 2a (open circles) and Fig. 2b (open squares) as a function of their width and that of the BC_3 sheet (dashed line).

Conclusions

In summary, the effect of enhanced π-conjugation has been studied for the case of armchair ribbons derived from a BC_3 sheet that presents a Kekulé-like structure with localised electron density on the carbon hexagons that are separated by sp^2-hybridised boron atoms. The removal of the passivating hydrogen atoms from the edge boron atoms results in sp-hybridisation, which leaves one π-electron unhybridised. This process enhances the π-conjugation along the edge, which results in higher stability and introduces a metallic density of states. All of these observations clearly indicate the sensitivity of edge passivation in low-dimensional materials. Interestingly, the increase in width gradually opens up a gap and results in an unusual metal to semiconductor transition. This phenomenon can be of great academic interest in the field of nanomaterials with possible applications in electronic devices with edge channels separated by a semiconducting bulk material.

Acknowledgements

S.D. acknowledges JSPS for postdoctoral fellowship and K.W. acknowledges the financial support by Grant-in-Aid for Scientific Research from the MEXT and the JSPS (nos. 23310083, 20001006).

Notes and references

1 K. S. Novoselov, *et al.*, *Proc. Natl. Acad. Sci. U. S. A.*, 2005, **102**, 10451; K. S. Novoselov, *et al.*, *Nature*, 2005, **438**, 197; Y. Zhang, Y. W. Tan, H. L. Stormer and P. Kim, *Nature*, 2005, **438**, 201.
2 T. Ando, *Prog. Theor. Phys., Suppl.*, 2008, **176**, 203.
3 A. H. Castro Neto, F. Guinea, N. M. R. Peres, K. S. Novoselov and A. K. Geim, *Rev. Mod. Phys.*, 2009, **81**, 109.
4 H. Nakano, *et al.*, *Angew. Chem., Int. Ed.*, 2006, **45**, 6303.
5 G. Le Lay, *et al.*, *Appl. Surf. Sci.*, 2009, **256**, 524; P. Vogt, *et al.*, *Phys. Rev. Lett.*, 2012, **108**, 155501.
6 W. Q. Han, L. Wu, Y. Zhu, K. Watanabe and T. Taniguchi, *Appl. Phys. Lett.*, 2008, **93**, 223103.
7 K. F. Mak, C. Lee, J. Hone, J. Shan and T. F. Heinz, *Phys. Rev. Lett.*, 2010, **105**, 136805; J. N. Coleman, *et al.*, *Science*, 2011, **331**, 568.
8 B. Radisavljevic, A. Radenovic, J. Brivio, V. Giacometti and A. Kis, *Nat. Nanotechnol.*, 2011, **6**, 147.
9 H. Tanaka, Y. Kawamata, H. Simizu, T. Fujita, H. Yanagisawa, S. Otani and C. Oshima, *Solid State Commun.*, 2005, **136**, 22; H. Yanagisawa, Y. Ishida, T. Tanaka, A. Ueno, S Otani and C. Oshima, *Surf. Sci.*, 2006, **600**, 4072.
10 H. Yanagisawa, T. Tanaka, Y. Ishida, E. Rokuta, S. Otani and C. Oshima, *Phys. Rev. B: Condens. Matter Mater. Phys.*, 2006, **73**, 045412; H. Yanagisawa, T. Tanaka, Y. Ishida, M. Matsue, E. Rokuta, S. Otani and C. Oshima, *Phys. Rev. Lett.*, 2004, **93**, 177003.
11 Y. Miyamoto, A. Rubio, S. G. Louie and M. L. Cohen, *Phys. Rev. B: Condens. Matter Mater. Phys.*, 1994, **50**, 18360.
12 D. Xiao, G. B. Liu, W. Feng, X. Xu and W. Yao, *Phys. Rev. Lett.*, 2012, **108**, 196802.
13 Z. Y. Zhu, Y. C. Cheng and U. Schwingenschlogl, *Phys. Rev. B: Condens. Matter Mater. Phys.*, 2011, **84**, 153402.

14 Z. Y. Meng, T. C. Lang, S. Wessel, F. F. Assaad and A. Muramatsu, *Nature*, 2010, **464**, 847.
15 H. Y. Hwang, *et al.*, *Nat. Mater.*, 2012, **11**, 103.
16 M. Osada and T. Sasaki, *J. Mater. Chem.*, 2009, **19**, 2503; M. Osada and T. Sasaki, *Adv. Mater.*, 2012, **24**, 210.
17 J. K. Ellis, M. J. Lucero and G. E. Scuseria, *Appl. Phys. Lett.*, 2011, **99**, 261908.
18 A. H. Castro Neto and K. S. Novoselov, *Mater. Express*, 2011, **1**, 10; A. H. Castro Neto and K. S. Novoselov, *Rep. Prog. Phys.*, 2011, **74**, 082501.
19 N. T. Cuong, M. Otani and S. Okada, *Phys. Rev. Lett.*, 2011, **106**, 106801.
20 C. R. Dean, *et al.*, *Nat. Nanotechnol.*, 2010, **5**, 722; C. R. Dean, *et al.*, *Nat. Phys.*, 2011, **7**, 693; A. F. Young, *et al.*, *Nat. Phys.*, 2012, **8**, 550.
21 K. S. Novoselov and A. H. Castro Neto, *Phys. Scr.*, 2012, **T146**, 014006.
22 M. Fujita, K. Wakabayashi, K. Nakada and K. Kusakabe, *J. Phys. Soc. Jpn.*, 1996, **65**, 1920.
23 K. Wakabayashi and S. Dutta, *Solid State Commun.*, 2012, **152**, 1420.
24 S. Dutta and S. K. Pati, *J. Mater. Chem.*, 2010, **20**, 8207.
25 C. Tao, *et al.*, *Nat. Phys.*, 2011, **7**, 616.
26 S. Dutta and K. Wakabayashi, *Sci. Rep.*, 2012, **2**, 519.
27 K. Wakabayashi, Y. Takane, M. Yamamoto and M. Sigrist, *New J. Phys.*, 2009, **11**, 095016.
28 Y. Miyamoto, K. Nakada and M. Fujita, *Phys. Rev. B: Condens. Matter Mater. Phys.*, 1999, **59**, 9858.
29 Y. W. Son, M. L. Cohen and S. G. Louie, *Phys. Rev. Lett.*, 2006, **97**, 216803.
30 We perform first principles calculations using the density functional package SIESTA [J. M. Soler, *et al.*, *J. Phys.: Condens. Matter*, 2002, **14**, 2745]. We consider generalized gradient approximation (GGA) and Perdew–Burke–Ernzerhof (PBE) exchange and correlation functional [J. P. Perdew, K. Burke and M. Ernzerhof, *Phys. Rev. Lett.*, 1996, **77**, 3865] for both spin non-polarized and polarized calculations with a double zeta polarized (DZP) basis set. Sufficient vacuum has been created in the non-periodic directions to avoid any interactions within adjacent unit cells. We consider 400 Ry energy cut-off for real space mesh size and a Brillouin zone sampling over $30 \times 30 \times 1$ and $70 \times 1 \times 1$ Monkhorst–Pack grid for the relaxation of two-dimensional BC_3 and ribbon structures, respectively, along with their lattice vectors until the force on each atom reaches 0.04 eV $Å^{-1}$. For electronic property calculations of optimized geometries, we consider the Brillouin zone sampling over $30 \times 30 \times 1$ and $300 \times 1 \times 1$ Monkhorst–Pack grid, respectively. Note that, the energy differences within the relaxed geometries with various initial spin orientation guesses are negligible with no total spin preference. Moreover, their electronic properties behave consistently. Therefore, we choose to present the results with initial antiferromagnetic spin orientation guess to be consistent with the graphene.
31 I. A. Popov and A. Boldyrev, *J. Phys. Chem. C*, 2012, **116**, 3147.
32 Q. Wang, L. Q. Chen and J. F. Annett, *Phys. Rev. B: Condens. Matter Mater. Phys.*, 1996, **54**, R2271.
33 D. Tomanek, R. M. Wentzcovitch, S. G. Louie and M. L. Cohen, *Phys. Rev. B: Condens. Matter Mater. Phys.*, 1988, **37**, 3134.
34 S. Dutta and S. K. Pati, *J. Phys. Chem. B*, 2008, **112**, 1333.
35 Y. Ding, Y. Wang and J. Ni, *Appl. Phys. Lett.*, 2009, **94**, 073111.

